Extended accuracy of coupled mode analysis for nanophotonic supercontinuum generation in multi-core waveguide structures

XINPENG CHEN[1], YONGYUAN CHU[1], KAILIN WU[1], MEIHUI ZENG[1], HONGYANG SHI[1], SUWAN SUN[1], AND HAIRUN GUO[1,*]

[1] *Key Laboratory of Specialty Fiber Optics and Optical Access Networks, Joint International Research Laboratory of Specialty Fiber Optics and Advanced Communication, Shanghai University, Shanghai 200444, China*
[*] *Corresponding author: hairun.guo@shu.edu.cn*

Compiled August 25, 2023

Waveguide design has always been an important part of photonic integrated devices, and its research is also developing. In this paper, the coupling between waveguides is studied from two aspects of coupled mode theory and finite element simulation. In addition, this paper gives an example of dispersion engineering caused by dual-core waveguides structure, which has a wide range of applications in supercontinuum. To sum up, coupled mode theory has important reference significance for the design of modern photonic devices.

http://dx.doi.org/10.1364/ao.XX.XXXXXX

1. INTRODUCTION

Evnascently light coupling among optical waveguides represents one of the most basic and applied effects in photonic circuits as well as in fiber optics, and have enabled a diversity of fundamental building blocks including directional couplers [1, 2], mode converters [3, 4], multiplexers [5, 6], interferometers [7], as well as resonators [8, 9], and have allowed for the observation of electromagnetically induced transparency [10, 11], integrated optical isolation [12], Parity-time symmetry [13], etc. In the phase matching condition, the light coupling would give rise to a number of distinct mode states as the superposition of individual modes, e.g. the pair of symmetric and anti-symmetric modes in a classic two-mode system. Such states are analogous to discrete energy states in molecular systems, and similar-to-molecule performances have been observed and controlled in photonics ways [14, 15]. On aspect of nonlinear photonics, such states have enabled advanced control of light in terms of the dispersion engineering [16, 17] and the nonlinear interaction.

Photonic supercontinuum generation is another scheme that could benefit from the light coupling effect, where localized dispersion engineering is enabled by induced dispersion of the mode coupling [18–20]. In particular the induced anomalous dispersion from the anti-symmetric mode is usually desired for soliton-regime supercontinuum, which could be designed at arbitrary wavelengths including the mid-infrared. Nevertheless the supercontinuum could also model a broadband and undepleted pumping system, where weak and localized mode couplings (i.e. coupling with higher-order modes or to higher-order harmonics) would feature resonant absorption and leave narrow line-shapes in the spectrum [21, 22], which again is analogous to molecular absorption usually featured in spectroscopy.

Recently, a mid-infrared dispersion engineered and flat supercontinuum has been successfully implemented in a dual-core coupled waveguide structure, and was further applied in a dual-comb spectrometer for parallel gas-phase detection [23]. Yet, the design process for such coupled waveguide structure is non-trivial. The most applied criterion is the coupled mode theory [24], which treats a coupled waveguide element (core) as dielectric disturbance, and predicts the light coupling dynamic on basis of individual modes (in individual waveguides). Indeed, the theory has been well studied and widely applied in the design of fundamental optical components, as well as recently in topological photonics [25, 26], photonic crystals [27, 28] and quantum cascade lasers [29]. Yet, the quantitative accuracy of the coupled mode theory remains questionable, especially towards the mid-infrared region where the mode confinement of the waveguide is reduced. As such, the modern way of performing the dispersion engineering is usually based on numerical simulations by means of e.g. the finite element method, which would certainly be more time-costing compared with the analytical method as repeated simulations are required to explore the waveguide dispersion on each structural parameter. This posts limitations to systematic.

In this letter, we rephrase the coupled mode theory, in which the coupling induced self-correction on the propagation constant is highlighted, and is understood as the key to extend the accuracy of the theory towards the cut-off (i.e. to the long wavelength range). With nonlinear effects, a revised coupled nonlinear Schrödinger equation is also derived. We then showcase the engineering of dispersion from the mode coupling, in the mid-infrared range in a photonic integrated dual-core waveg-

uide, which has excellent accuracy and could be applied in the prediction of mid-infrared supercontinuum generation including the dispersive wave generation.

2. THEORETICAL MODEL

Here, we limit the coupled mode analysis regarding the most typical waveguide structure, namely the structure with two parallel waveguide cores. The coupling of mode amplitudes ($a(z)$ and $b(z)$) in individual cores , along the propagation axis (z), are generally described as:

$$\begin{cases} \frac{da(z)}{dz} = -i\kappa_{ab} b e^{i\Delta\beta z} \\ \frac{db(z)}{dz} = -i\kappa_{ba} a e^{-i\Delta\beta z} \end{cases} \tag{1}$$

where κ_{ab} and κ_{ba} are the exchange coupling coefficients between the modes, and $\Delta\beta$ indicates the phase mismatch. The complete form of Eq. 1 could be derived based on the dielectric perturbation theory. In this context, the electric field of the general wave in the dual-core waveguide can be approximated by:

$$E(x,y,z,t) = a(z)E_a(x,y)e^{i[\omega t-(\beta_a-\kappa_{aa})z]} + b(z)E_b(x,y)e^{i[\omega t-(\beta_b-\kappa_{bb})z]} \tag{2}$$

where $E_{a,b}(x,y)$ indicates the transverse mode field distribution. It should be noted that a self-correction factor (i.e. κ_{aa} or κ_{bb}) is introduced, which physically is resulted by dielectric perturbations to one of the modes due to the presence of the other one.

In principle, the electric field given by Eq. 2 must obey the wave equation

$$\left(\frac{\partial^2}{\partial x^2} + \frac{\partial^2}{\partial y^2} + \frac{\partial^2}{\partial z^2} + \frac{\omega^2}{c^2}\ n^2(x,y)\right) E = 0 \tag{3}$$

where the refractive index (ri) distribution is further expanded as: $n^2(x,y) = n_s^2(x,y) + \Delta n_a^2(x,y) + \Delta n_b^2(x,y)$ (n_s is defined as the ri of the substrate or cladding area outside the waveguide cores, and $\Delta n_{a,b}^2$ indicates the difference of squared ri of the core to that of the substrate. Thus, Eq. 3 can be expanded, and a dynamic with respect to the mode amplitude $a(z)$ is obtained as: (similar for the dynamic of $b(z)$)

$$\begin{aligned} \frac{da}{dz} &= -ia(\kappa_{aa} - \tfrac{\omega\varepsilon_0}{4}\iint \Delta n_b^2(x,y)E_a E_a^* dxdy) \\ &-ib\tfrac{\omega\varepsilon_0}{4}\iint \Delta n_a^2(x,y)E_b E_a^* dxdy \end{aligned} \tag{4}$$

where ε_0 is vacuum permittivity.

To force a consistent form with Eq. 1, one could conclude the coupling coefficients, the self-correction factors, and the phase mismatch as the following:

$$\begin{cases} \kappa_{ab} = \frac{\omega\varepsilon_0}{4}\iint \Delta n_a^2(x,y)E_b E_a^* dxdy \\ \kappa_{ba} = \frac{\omega\varepsilon_0}{4}\iint \Delta n_b^2(x,y)E_a E_b^* dxdy \\ \kappa_{aa} = \frac{\omega\varepsilon_0}{4}\iint \Delta n_b^2(x,y)E_a E_a^* dxdy \\ \kappa_{bb} = \frac{\omega\varepsilon_0}{4}\iint \Delta n_a^2(x,y)E_b E_b^* dxdy \\ \Delta\beta = (\beta_a - \kappa_{aa}) - (\beta_b - \kappa_{bb}) \end{cases} \tag{5}$$

We further make $A = \sqrt{\kappa_{ba}}ae^{-i(\beta_a-\kappa_{aa})z}$ and $B = \sqrt{\kappa_{ab}}be^{-i(\beta_b-\kappa_{bb})z}$. So a set of coupled mode equations is derived as:

$$\begin{bmatrix} \frac{dA}{dz} \\ \frac{dB}{dz} \end{bmatrix} = -i\begin{bmatrix} (\beta_a - \kappa_{aa}) & \kappa \\ \kappa & (\beta_b - \kappa_{bb}) \end{bmatrix}\begin{bmatrix} A \\ B \end{bmatrix} \tag{6}$$

where the renewed coupling coefficient $\kappa = \sqrt{\kappa_{ab}\kappa_{ba}}$ naturally form a complex conjugate pair in the transfer matrix. As such the energy conservation is ensured for the coupling between A and B.

Moreover, the eigenvalue(s) of the transfer matrix could be calculated, i.e.:

$$\lambda_{1,2} = \frac{(\beta_a - \kappa_{aa}) + (\beta_b - \kappa_{bb})}{2} \pm \frac{S}{2} \tag{7}$$

where $S = \sqrt{\Delta\beta^2 + 4\kappa^2}$. The eigenvectors are:

$$\tilde{e}_1 = \begin{bmatrix} \frac{2\kappa}{\Delta\beta+s} \\ 1 \end{bmatrix}, \tilde{e}_2 = \begin{bmatrix} \frac{2\kappa}{\Delta\beta-s} \\ 1 \end{bmatrix} \tag{8}$$

Physically, such eigenvalues are comparative with the propagation constants of the symmetric and anti-symmetric modes in the dual-core waveguide, and the elements in eigenvectors indicates the amplitude of individual modes (A and B) in forming such superpositioned modes (supermodes).

To facilitate the simulation of nonlinear pulse propagation and supercontinuum generation in such a coupled dual-core waveguide system, Eq. 6 is further extended to contain the nonlinear phase modulation effects, forming a set of coupled nonlinear Schrödinger equations (NLSEs), i.e.:

$$\begin{cases} \frac{dA'}{dz} = -i(\beta_a - \kappa_{aa} - \beta_s)A' - i\kappa B' - i\gamma_a F\left[|A'|^2 A'\right] \\ \frac{dB'}{dz} = -i(\beta_b - \kappa_{bb} - \beta_s)B' - i\kappa A' - i\gamma_b F\left[|B'|^2 B'\right] \end{cases} \tag{9}$$

where a dispersionless phase constant β_s is assumed underlying the mode amplitude, i.e. $A' = Ae^{-i\beta_s z}$ and $B' = Be^{-i\beta_s z}$, $\beta_s = \beta_a(\omega_s) + (\omega - \omega_s)v_g^{-1}$ (ω_s is the central angular frequency of the pumping pulse, and v_g is a referenced group velocity of the pulse), $\gamma_{a,b}$ indicates the nonlinear coefficient for the self-phase modulation, which is dependent on the effective mode area ($A_{\text{eff }a,b}$) in individual waveguide cores, i.e. $\gamma_{a,b} \propto A_{\text{eff }a,b}^{-1}$.

Compared with the conventional NLSE, a primary change of Eq. 9 is the presence of the self-correction coefficients, which may impact the dispersion profile and lead to deviations on the nonlinear pulse propagation dynamic, including the pulse seeding supercontinuum process.

3. RESULTS

A. Symmetrical double waveguides

For dual-core waveguide structure as shown in Fig1.(a) (h=1000 nm, w=1000 nm, g=1000 nm; $n_{a,b} = n_{Si_3N_4}$, $n_s = n_{SiO_2}$). When the same waveguides are closer, the optical mode propagating in one will be coupled to the other, which effectively changes its phase i.e. the propagation constant($\beta(\lambda)$, λ is the wavelength of the light). Physically, mode coupling will bring the hybridization of mode-field distributions, resulting in a pair of supermodes, namely the symmetric and anti-symmetric modes.

Usually, the propagation constants of super modes $\beta_{s1,s2}$ can be calculated by COMSOL simulation. However, the eigenvalues $\lambda_{1,2}$ solved by the Eq. 7 can also be used as the propagation constant of super modes. In order to study the influence of coupling, uniformly observe the change of propagation constants. Through data processing, it is found that the contrast satisfies the following relationship $\beta_{s1} - \beta_b = \lambda_1 - \beta_b, \beta_{s2} - \beta_a = \lambda_2 - \beta_a$,

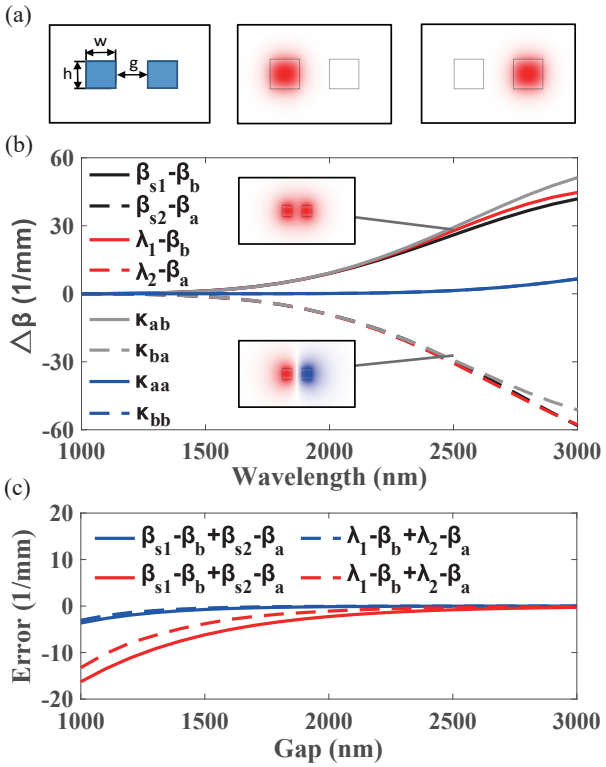

Fig. 1. Coupling between the same waveguides. (a) Design of dual-core waveguide structure: h is height, w is width, and g is the gap between two waveguides. (b) Comparison of propagation constant changes; Inset is the electric filed distribution of super modes s1 and s2. (c) Error caused by changing the gap. The blue line and red line represent 2500 nm and 3000 nm wavelength positions respectfully.

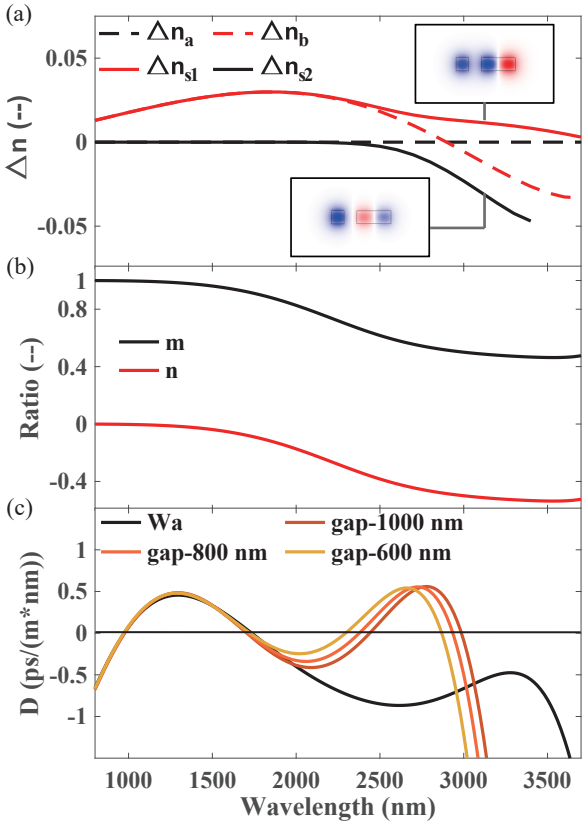

Fig. 2. Coupling between 2 different waveguides. (a) Relative effective refractive index difference of super modes s1,s2 and single waveguide a,b calculated based on waveguide a; (b) Coefficients obtained from eigenvectors for synthesizing supermodel electric fields. (c) Dispersion calculation of independent waveguide a and dual-core waveguide structure with different gaps.

which can be clearly observed in Fig1.(b). In addition, the obtained self coupling coefficient is very small whose effect on the propagation constant usually be neglected. In fact, if do not make the $\beta_a - \kappa_{aa}$ for correction as mentioned in Eq. 2, $\lambda_1 - \beta_b$ will directly equal to κ_{ab} which will bring the inaccuracy as shown in Fig1.(b).

By changing the gap between two waveguides to smaller, as shown in Fig1.(c), it is found that the relative difference of the relationship will gradually increase. Especially, the asymmetry results of two supermodes in this structure will become more and more obvious at the long wavelength, which can be explained by the existing of self coupling coefficient.

B. Asymmetric double waveguides

Since different waveguides with different propagation constants, 2 suitable waveguides that exist the coupling should be selected. As shown in Fig2.(a), the start wavelength of the coupling and the phase matching point of the dual-core waveguide structure can be easily found by calculating the relative effective refractive index($\Delta n_i = n_i - n_a$). Finally the designed waveguide a and b can be determined(width of a is 1000 nm, b is 3000 nm and g=1000 nm, h=1000 nm).

At the same time, described as $\triangle n_{s2}$ in Fig2.(a), the appearance of anomalous dispersion caused by coupling can be easily observed. In addition, Fig2.(b) shows the variation value of 2 independent electric field composition which is related to the eigenvector mentioned in Eq. 8. For example $E_s = m \cdot E_a + n \cdot E_b$, where $|m| + |n| = 1$. Especially, when two waveguides are the same, $|m| = |n|$. Besides, for dispersion engineering, changing the gap can adjust the region of anomalous dispersion as shown in Fig2.(c).

For supercontinuum generation, Fig3.(a) shows the change of relative propagation constant of 2 independent waveguides and dual-core waveguide structure which are calculated by COMSOL simulation. In Fig3.(b), pumping waveguide a at 2000 nm, the supercontinuum spectrum after coupling can be achieved from Eq. 9. Besides, the comparison between simulation and theoretical calculation of supercontinuum generation also be given in Fig3.(c). Especially, the grey line gives the result of without self-correction factor (i.e. κ_{aa} or κ_{bb}).

According to the supercontinuum, although there are some differences, the correction of introducing the self-correction factor is necessary, which can be observed especially from the position of the dispersive wave. Importantly, we can draw a conclusion that when designing waveguides based on coupled mode theory will not only improve the accuracy but also speed up the calculation.

4. CONCLUSION

From the comparison results, we can get some meaningful conclusions. First, since waveguide modes tend to be cut off at

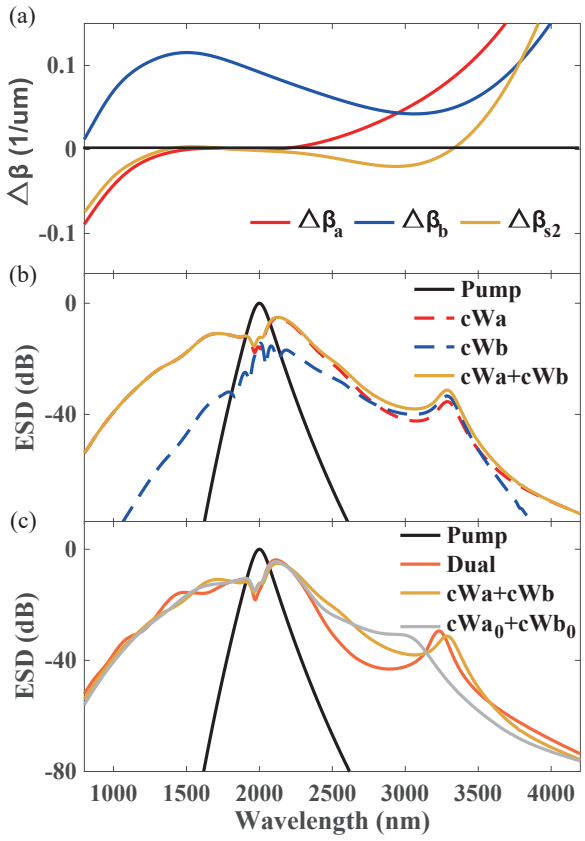

Fig. 3. Supercontinuum generation. (a) Calculated dispersion landscape of the anti-symmetric mode of dual-core waveguide structure (gap = 600 nm) and the fundamental mode of waveguide a,b. (b) Supercontinuum generated by two independent waveguides based on coupled mode theory. (c) Comparison of supercontinuum generation based on coupled mode theory and software simulation.

long wavelength, using the coupled mode theory can effectively avoid the errors caused by simulation; Second, the inconsistency of the calculated supermodes for the dual-core waveguide structure of the same waveguides can be explained by the existence of self coupling coefficient.

Last but not least, we focus on the coupling between 2 different waveguides which can bring abnormal dispersion for dispersion engineering. And we find the differences between theoretical calculation and simulation calculation, especially the effect of self coupling coefficient. Nevertheless, we know the difference between the supercontinuum spectrum generated by the two methods, and we can use it for reference in the future waveguide design work.

Funding. National Natural Science Foundation of China (11974234); National Key Research and Development Program of China (2020YFA0309400); Shanghai Science and Technology Development Foundation (20QA1403500).

Acknowledgments. We acknowledge funding from National Natural Science Foundation of China (No. 11974234), Shanghai Science and Technology Development Funds (No. 20QA1403500), and National Key Research and Development Project of China (No. 2020YFA0309400).

Disclosures. The authors declare no conflicts of interest.

Data Availability Statement. A Data Availability Statement (DAS) will be required for all submissions beginning 1 March 2021. The DAS should be an unnumbered separate section titled "Data Availability" that immediately follows the Disclosures section. See the Data Availability Statement policy page for more information.

REFERENCES

1. T. Y. Teo, M. Krbal, J. Mistrik, J. Prikryl, L. Lu, and R. E. Simpson, Opt. Mater. Express **12**, 606 (2022).
2. B. Bhandari and S.-S. Lee, Sci. Reports **12**, 7252 (2022).
3. B. Sun, F. Morozko, P. S. Salter, S. Moser, Z. Pong, R. B. Patel, I. A. Walmsley, A. Hazan, N. BarrÃľ, A. Jesacher, J. Fells, A. Katiyi, A. Novitsky, A. Karabchevsky, and M. J. Booth, Light. Sci. & Appl. **11**, 214 (2022).
4. X. Shu, A. Li, G. Hu, J. Wang, A. AlÃź, and L. Chen, Nat. Commun. **13**, 2123 (2022).
5. T. Fujisawa, J. Takano, Y. Sawada, and K. Saitoh, J. Light. Technol. **39**, 193 (2021).
6. Y. Cao, K. Nallappan, G. Xu, and M. Skorobogatiy, Nat. Commun. **13**, 4090 (2022).
7. M. Nedeljkovic, J. S. Penades, C. J. Mitchell, A. Z. Khokhar, S. Stankovic, T. D. Bucio, C. G. Littlejohns, F. Y. Gardes, and G. Z. Mashanovich, IEEE Photonics Technol. Lett. **27**, 1040 (2015).
8. C. Chen, S.-H. Oh, and M. Li, Opt. Express **28**, 2020 (2020).
9. D. Liu, J. He, Y. Xiang, Y. Xu, and D. Dai, APL Photonics **7**, 051303 (2022).
10. T. Wang, T. Li, H. Yao, Y. Lu, X. Yan, M. Cao, L. Liang, M. Yang, and J. Yao, Photonics Res. **10**, 2317 (2022).
11. W. Xu, Z. Yang, H. Zhou, Y. Wu, H. Zhu, X. Zhang, and B.-X. Wang, Phys. Scripta **97**, 065509 (2022).
12. H. Tian, J. Liu, A. Siddharth, R. N. Wang, T. BlÃľsin, J. He, T. J. Kippenberg, and S. A. Bhave, Nat. Photonics **15**, 828 (2021).
13. X. Lu, N. Chen, B. Zhang, H. Yang, Y. Chen, X. Zhang, and J. Xu, arXiv e-prints arXiv:2204.11556 (2022).
14. S. Kapfinger, T. Reichert, S. Lichtmannecker, K. MÃijller, J. J. Finley, A. Wixforth, M. Kaniber, and H. J. Krenner, Nat. Commun. **6**, 8540 (2015).
15. M. Zhang, C. Wang, Y. Hu, A. Shams-Ansari, T. Ren, S. Fan, and M. Lončar, Nat. Photonics **13**, 36 (2019).
16. S. Kim, K. Han, C. Wang, J. A. Jaramillo-Villegas, X. Xue, C. Bao, Y. Xuan, D. E. Leaird, A. M. Weiner, and M. Qi, Nat. Commun. **8**, 372 (2017).
17. Ã. B. Helgason, F. R. Arteaga-Sierra, Z. Ye, K. Twayana, P. A. Andrekson, M. Karlsson, J. SchrÃűder, and Victor Torres-Company, Nat. Photonics **15**, 305 (2021).
18. L. Zhang, Q. Lin, Y. Yue, Y. Yan, R. G. Beausoleil, and A. E. Willner, Opt. Express **20**, 1685 (2012).
19. D. D. Hickstein, H. Jung, D. R. Carlson, A. Lind, I. Coddington, K. Srinivasan, G. G. Ycas, D. C. Cole, A. Kowligy, C. Fredrick, S. Droste, E. S. Lamb, N. R. Newbury, H. X. Tang, S. A. Diddams, and S. B. Papp, Phys. Rev. Appl. **8**, 014025 (2017).
20. S. Fatema, M. B. Mia, and S. Kim, J. Light. Technol. **39**, 216 (2021).
21. D. D. Hickstein, G. C. Kerber, D. R. Carlson, L. Chang, D. Westly, K. Srinivasan, A. Kowligy, J. E. Bowers, S. A. Diddams, and S. B. Papp, Phys. Rev. Lett. **120**, 053903 (2018).
22. H. Chen, J. Zhou, D. Li, D. Chen, A. K. Vinod, H. Fu, X. Huang, T.-H. Yang, J. A. Montes, K. Fu, C. Yang, C.-Z. Ning, C. W. Wong, A. M. Armani, and Y. Zhao, ACS Photonics **8**, 1344 (2021).
23. H. Guo, W. Weng, J. Liu, F. Yang, W. Hansel, C. S. Bres, L. Thevenaz, R. Holzwarth, and T. J. Kippenberg, Optica **7**, 1181 (2020).
24. R. G. Hunsperger, *Integrated Optics* (Springer New York, New York, NY, 2009).
25. Q. Cheng, S. Wang, J. Lv, and N. Liu, Opt. Express **30**, 10792 (2022).
26. J. Chen and Y. Fan, Opt. Commun. **505**, 127530 (2022).
27. S. Elshahat, Z. E. A. Mohamed, M. Almokhtar, and C. Lu, J. Opt. **24**, 035004 (2022).
28. X. Letartre, S. Mazauric, S. Cueff, T. Benyattou, H. S. Nguyen, and P. Viktorovitch, Phys. Rev. A **106**, 033510 (2022). ArXiv:2203.05226 [physics].

29. J. Li, F. Sun, Y. Jin, Y. D. Chua, K. H. Tan, S. Wicaksono, C. Sirtori, S. F. Yoon, and Q. J. Wang, Opt. Express **30**, 629 (2022).

FULL REFERENCES

1. T. Y. Teo, M. Krbal, J. Mistrik, J. Prikryl, L. Lu, and R. E. Simpson, "Comparison and analysis of phase change materials-based reconfigurable silicon photonic directional couplers," Opt. Mater. Express **12**, 606 (2022).
2. B. Bhandari and S.-S. Lee, "Reconfigurable fiber-to-waveguide coupling module enabled by phase-change material incorporated switchable directional couplers," Sci. Reports **12**, 7252 (2022).
3. B. Sun, F. Morozko, P. S. Salter, S. Moser, Z. Pong, R. B. Patel, I. A. Walmsley, A. Hazan, N. BarrÃľ, A. Jesacher, J. Fells, A. Katiyi, A. Novitsky, A. Karabchevsky, and M. J. Booth, "On-chip beam rotators, adiabatic mode converters, and waveplates through low-loss waveguides with variable cross-sections," Light. Sci. & Appl. **11**, 214 (2022).
4. X. Shu, A. Li, G. Hu, J. Wang, A. AlÃź, and L. Chen, "Fast encirclement of an exceptional point for highly efficient and compact chiral mode converters," Nat. Commun. **13**, 2123 (2022).
5. T. Fujisawa, J. Takano, Y. Sawada, and K. Saitoh, "Low-Loss and Small $2\times4\lambda$ Multiplexers Based on 2×2 and 2×1 MachâĂŞZehnder Interferometers With On-Chip Polarization Multiplexing for 400GbE," J. Light. Technol. **39**, 193–200 (2021).
6. Y. Cao, K. Nallappan, G. Xu, and M. Skorobogatiy, "Add drop multiplexers for terahertz communications using two-wire waveguide-based plasmonic circuits," Nat. Commun. **13**, 4090 (2022).
7. M. Nedeljkovic, J. S. Penades, C. J. Mitchell, A. Z. Khokhar, S. Stankovic, T. D. Bucio, C. G. Littlejohns, F. Y. Gardes, and G. Z. Mashanovich, "Surface-Grating-Coupled Low-Loss Ge-on-Si Rib Waveguides and Multimode Interferometers," IEEE Photonics Technol. Lett. **27**, 1040–1043 (2015).
8. C. Chen, S.-H. Oh, and M. Li, "Coupled-mode theory for plasmonic resonators integrated with silicon waveguides towards mid-infrared spectroscopic sensing," Opt. Express **28**, 2020 (2020).
9. D. Liu, J. He, Y. Xiang, Y. Xu, and D. Dai, "High-performance silicon photonic filters based on all-passive tenth-order adiabatic elliptical-microrings," APL Photonics **7**, 051303 (2022).
10. T. Wang, T. Li, H. Yao, Y. Lu, X. Yan, M. Cao, L. Liang, M. Yang, and J. Yao, "High-sensitivity modulation of electromagnetically induced transparency analog in a THz asymmetric metasurface integrating perovskite and graphene," Photonics Res. **10**, 2317 (2022).
11. W. Xu, Z. Yang, H. Zhou, Y. Wu, H. Zhu, X. Zhang, and B.-X. Wang, "Triple-band electromagnetically induced transparency effects enabled by two sets of arc-ring-type resonators at terahertz frequency," Phys. Scripta **97**, 065509 (2022).
12. H. Tian, J. Liu, A. Siddharth, R. N. Wang, T. BlÃľsin, J. He, T. J. Kippenberg, and S. A. Bhave, "Magnetic-free silicon nitride integrated optical isolator," Nat. Photonics **15**, 828–836 (2021).
13. X. Lu, N. Chen, B. Zhang, H. Yang, Y. Chen, X. Zhang, and J. Xu, "Design optimization of band-pass filter based on parity-time symmetry coupled-resonant," arXiv e-prints arXiv:2204.11556 (2022).
14. S. Kapfinger, T. Reichert, S. Lichtmannecker, K. MÃijller, J. J. Finley, A. Wixforth, M. Kaniber, and H. J. Krenner, "Dynamic acousto-optic control of a strongly coupled photonic molecule," Nat. Commun. **6**, 8540 (2015).
15. M. Zhang, C. Wang, Y. Hu, A. Shams-Ansari, T. Ren, S. Fan, and M. Lončar, "Electronically programmable photonic molecule," Nat. Photonics **13**, 36–40 (2019).
16. S. Kim, K. Han, C. Wang, J. A. Jaramillo-Villegas, X. Xue, C. Bao, Y. Xuan, D. E. Leaird, A. M. Weiner, and M. Qi, "Dispersion engineering and frequency comb generation in thin silicon nitride concentric microresonators," Nat. Commun. **8**, 372 (2017).
17. Ã. B. Helgason, F. R. Arteaga-Sierra, Z. Ye, K. Twayana, P. A. Andrekson, M. Karlsson, J. SchrÃűder, and Victor Torres-Company, "Dissipative solitons in photonic molecules," Nat. Photonics **15**, 305–310 (2021).
18. L. Zhang, Q. Lin, Y. Yue, Y. Yan, R. G. Beausoleil, and A. E. Willner, "Silicon waveguide with four zero-dispersion wavelengths and its application in on-chip octave-spanning supercontinuum generation," Opt. Express **20**, 1685 (2012).
19. D. D. Hickstein, H. Jung, D. R. Carlson, A. Lind, I. Coddington, K. Srinivasan, G. G. Ycas, D. C. Cole, A. Kowligy, C. Fredrick, S. Droste, E. S. Lamb, N. R. Newbury, H. X. Tang, S. A. Diddams, and S. B. Papp, "Ultrabroadband Supercontinuum Generation and Frequency-Comb Stabilization Using On-Chip Waveguides with Both Cubic and Quadratic Nonlinearities," Phys. Rev. Appl. **8**, 014025 (2017).
20. S. Fatema, M. B. Mia, and S. Kim, "Multiple Mode Couplings in a Waveguide Array for Broadband Near-Zero Dispersion and Supercontinuum Generation," J. Light. Technol. **39**, 216–222 (2021).
21. D. D. Hickstein, G. C. Kerber, D. R. Carlson, L. Chang, D. Westly, K. Srinivasan, A. Kowligy, J. E. Bowers, S. A. Diddams, and S. B. Papp, "Quasi-Phase-Matched Supercontinuum Generation in Photonic Waveguides," Phys. Rev. Lett. **120**, 053903 (2018).
22. H. Chen, J. Zhou, D. Li, D. Chen, A. K. Vinod, H. Fu, X. Huang, T.-H. Yang, J. A. Montes, K. Fu, C. Yang, C.-Z. Ning, C. W. Wong, A. M. Armani, and Y. Zhao, "Supercontinuum Generation in High Order Waveguide Mode with near-Visible Pumping Using Aluminum Nitride Waveguides," ACS Photonics **8**, 1344–1352 (2021).
23. H. Guo, W. Weng, J. Liu, F. Yang, W. Hansel, C. S. Bres, L. Thevenaz, R. Holzwarth, and T. J. Kippenberg, "Nanophotonic supercontinuum based mid-infrared dual-comb spectroscopy," Optica **7**, 1181 (2020).
24. R. G. Hunsperger, *Integrated Optics* (Springer New York, New York, NY, 2009).
25. Q. Cheng, S. Wang, J. Lv, and N. Liu, "Topological photonic crystal biosensor with valley edge modes based on a silicon-on-insulator slab," Opt. Express **30**, 10792 (2022).
26. J. Chen and Y. Fan, "Topological BlochâĂŞZener oscillations in non-Hermitian graphene plasmonic waveguide arrays," Opt. Commun. **505**, 127530 (2022).
27. S. Elshahat, Z. E. A. Mohamed, M. Almokhtar, and C. Lu, "High tunability and sensitivity of 1D topological photonic crystal heterostructure," J. Opt. **24**, 035004 (2022).
28. X. Letartre, S. Mazauric, S. Cueff, T. Benyattou, H. S. Nguyen, and P. Viktorovitch, "Analytical non-Hermitian description of Photonic Crystals with arbitrary Lateral and Transverse symmetry," Phys. Rev. A **106**, 033510 (2022). ArXiv:2203.05226 [physics].
29. J. Li, F. Sun, Y. Jin, Y. D. Chua, K. H. Tan, S. Wicaksono, C. Sirtori, S. F. Yoon, and Q. J. Wang, "Widely tunable single-mode slot waveguide quantum cascade laser array," Opt. Express **30**, 629 (2022).